

Observational predictions of some inflationary models

Daniel Pozo¹, Lenin Calvache¹, Esteban Orozco¹, Clara Rojas¹

Abstract

This paper presents the CMB angular power spectrum obtained using the **CAMB** code for three different models of inflation: the Starobinsky inflationary model, the generalized Starobinsky inflationary model, and the chaotic inflationary model with a step. The results are compared with the most recent data reported for the Planck mission. An analysis of the large ($l \lesssim 90$), intermediate ($90 \lesssim l \lesssim 900$), and small ($l \gtrsim 900$) angular scales is performed. We report the position of the peaks in the intermediate region so as the cosmological parameters obtained in each of the models: age of the universe, Ω_m , Ω_b , Ω_Λ , Ω_K and n_S .

Keywords:

CMB angular power spectrum, **CAMB** code, Starobinsky inflationary model, generalized Starobinsky inflationary model, chaotic inflationary model with a step.

1. Introduction

The Big Bang theory describes the development of the Universe from a much hotter and denser point to the present. It is supported by solid observational evidence: the expansion of the Universe, the prediction of light element abundances, and the existence of the Cosmic Microwave Background (CMB) radiation. The CMB is a picture of the recombination epoch (370,000 years after the big bang). The first prediction of the CMB was made by Alpher and Herman in 1948 [1], and was discovered in 1965 by Penzias and Wilson [2]. It became one of the most important observational probes of the Big-bang theory. The CMB is an almost uniform and isotropic radiation field and shows a perfect black body spectrum at a temperature of 2.72K [3].

Email address: daniel.pozo@yachaytech.edu.ec (Daniel Pozo)

The CMB has fluctuations in a part of 10^5 that give rise to the structure of the present Universe [4].

Although the big bang theory stands as a robust and widely accepted explanation for the beginning of our Universe, this theory has three problems related to its initial conditions, the flatness problem, the horizon problem, and the monopole problem. To address these concerns, Alan Guth introduced the inflationary theory in 1981 [5]. This theory proposes an epoch of accelerated expansion preceding the hot stage mentioned in the traditional Big Bang model. The simplest possibility to produce such epoch is via the potential energy of a scalar field, and the field ϕ is called the inflaton. There are several inflationary models with their own scalar potentials, and through the years studies on which of them are favored by the satellites data have been made [6, 7, 8, 9]. One notable outcome of inflation is that provides a mechanism to generate the primordial scalar perturbations and produce an almost scale invariant scalar power spectrum.

The accurate recreation of the angular power spectrum can judge how well an inflationary theoretical model works to describe our early Universe, in this work this recreation is made using the **CAMB** code [10, 11]. The recent report by the Planck mission favors the models with a low amount of tensor perturbations i.e., small values of tensor-to-scalar ratio [12]. For this reason, the Starobinsky inflationary model [13] has become an important candidate, however a slight variation of the Starobinsky inflationary model that depends on a parameter p close to the unity improved our results [14, 15, 16]. Recently, Di Valentino and Mersini-Houghton [17] have studied the CMB angular power spectra for the modified Starobinsky potential in the context of the quantum landscape multiverse using a modified **CAMB** code.

We also analyze the chaotic inflationary model with a step, which has been caused of interest in recent years [18, 19, 20, 21, 22]. Adams and Cresswell [22], influenced by the existence of potentials that lead to scale dependent spectra, studied the consequences of introducing a step in the quadratic potential of the chaotic inflationary model, $V(\phi) = \frac{1}{2}m^2\phi^2$. Adding “features” to the potential can produce scale dependence in the primordial perturbation spectra [22].

Using the **CAMB** code we study for each model the three regions of the CMB angular power spectrum: a) the Sachs–Wolfe plateau region ($\ell < 90$) which correspond to large angular scales ($\theta > 2^\circ$), b) the acoustic peak region ($90 < \ell < 900$), and c) the silk damping region ($\ell > 900$). It is important to note that Macorra *et al.* have used the **CAMB** code with full **COSMO--MC**

(MCMC) calculation tzo give a solution to one of the most recent conflicts in Modern Cosmology: the Hubble tension [23]. Also, Purkayastha et al. have estimate CMB E mode signal over large angular scales [24].

To study CMB, we utilize the radiation angular power spectrum, which is both measurable and theoretically predictable. The radiation angular power spectrum C_ℓ is defined by:

$$C_\ell = \{|a_{\ell m}|^2\}, \quad (1)$$

where $a_{\ell m}$ are the coefficients of the expansion in spherical harmonics

$$\frac{\Delta T}{T}(\theta, \phi) = \sum_{\ell=1}^{\infty} \sum_{m=-\ell}^{\ell} a_{\ell m} Y_m^\ell(\theta, \phi), \quad (2)$$

of a dimensionless temperature anisotropy, which is given by

$$\frac{\Delta T}{T}(\theta, \phi) = \frac{T(\theta, \phi) - \bar{T}}{\bar{T}}, \quad (3)$$

where $T(\theta, \phi)$ is the microwave background temperature measured in some direction on the sky and \bar{T} the mean temperature.

C_ℓ depends only of ℓ since the statistical properties are required to be independent of the choice of the origin of $\theta - \phi$, that is rotational invariance, or from a physical point of view, isotropy [25]. The larger is ℓ , the smaller is the angular scale at which the spherical harmonics have variation [26].

Also (and it is the case for this article), the C_ℓ spectrum is conventionally plotted as $\ell(\ell + 1)C_\ell \bar{T}^2 / 2\pi$, measuring the power per logarithmic interval in ℓ . In such plot, a scale-invariant spectrum looks horizontal [25].

Using the **CAMB** code we study, for each model, the three regions of the CMB angular power spectrum:

1.1. The Sachs–Wolfe plateau region ($\ell < 90$)

At this scale (large scale), also called the horizon scale, anisotropies reflect the initial conditions since they have not evolved significantly.

Assuming a nearly scale-invariant spectrum of density perturbations in early times ($n_S \approx 1$), meaning gravitational potential fluctuations that are independent of k , then $\ell(\ell + 1)C_\ell$ remains constant at low ℓ_S . This effect is more evident when the multipole axis is plotted logarithmically, as did in this article.

Time variation in potentials, associated with time-dependent metric perturbations, causes an increase in the $C_{\ell S}$ at the lowest multipoles, influenced by any deviation from a total equation of state $w = 0$. The Dark Energy's dominance at low redshift causes the lowest ℓ s to rise above the plateau, known as the ‘integrated Sachs–Wolfe effect’ or ISW Rise, confirmed through correlations between large-angle anisotropies and large-scale structure.

In summary, the mechanism generating primordial perturbations produces scalar, vector, and tensor modes. While vector modes and tensors decay with the expansion of the Universe, their contribution to the low ℓ signal, especially gravity waves, can be challenging to distinguish from other effects. However, polarization information can help differentiate tensor modes [27].

1.2. The acoustic peak region ($90 < \ell < 900$)

The intricate patterns observed in the anisotropy spectrum on intermediate scales can be attributed to gravity-driven acoustic oscillations that occurred prior to the neutralization of atoms in the universe. The frozen-in phases of these sound waves leave an imprint on cosmological parameters, lending significant constraining power to the anisotropies in the CMB.

During the era when the proton–electron plasma was closely coupled to photons, both components behaved as a unified ‘photon–baryon fluid’, wherein photons contributed primarily to pressure, and baryons imparted inertia. Gravitational potential perturbations, dominated by dark matter, drove oscillations in this fluid, with photon pressure acting as the restoring force. Despite their small amplitude ($\mathcal{O}(10^{-5})$), these perturbations evolved linearly, treating each Fourier mode independently as a driven harmonic oscillator. The frequency of these oscillations was determined by the sound speed in the fluid, resulting in a fluid density oscillation with a velocity out of phase and reduced amplitude.

Following the recombination of baryons and the decoupling of radiation, allowing photons to travel freely, the oscillation phases were frozen-in. Projected onto the sky, these frozen-in phases manifested as a harmonic series of peaks. The primary peak represented the mode that completed $1/4$ of a period, reaching maximal compression. Even peaks denoted maximal underdensities, typically of smaller amplitude due to the rebound having to overcome baryon inertia. Troughs, not reaching zero power, were partially filled as they corresponded to velocity maxima [27].

1.3. The silk damping region ($\ell > 900$)

The last scattering surface acquires a non-instantaneous thickness due to the recombination process, resulting in a damping effect on anisotropies at higher ℓ 's. This damping is particularly noticeable on scales smaller than the thickness of the last scattering surface. Another perspective is to view the photon–baryon fluid as having imperfect coupling, leading to diffusion between the two components and a gradual reduction in the amplitudes of oscillations over time. These effects collectively contribute to a phenomenon known as Silk damping, effectively truncating the anisotropies at multipoles exceeding approximately 2000 [27].

The paper is organized as follows: in Section 2 we define the slow-roll parameters and we describe how to calculate the cosmological parameters into the slow-roll approximation. Sections 3, 4, and 5 are devoted to calculating the CMB angular power spectrum obtained from `CAMB` for the Starobinsky inflationary model, the generalized Starobinsky inflationary model, and the chaotic inflationary model with a step. Finally, the conclusions are discussed in Section 6.

2. Slow-roll approximation and cosmological parameters

The slow-roll approximation is a standard technique in inflationary cosmology to solve the movement equations and the scalar and tensor equation of perturbations. This approximation is characterized by a set of parameters that establish when the approximation is valid or not and are given in terms of the inflationary potential and its derivatives in the following way [28, 29]

$$\epsilon_\nu = \frac{1}{2} \left(\frac{V'}{V} \right)^2, \quad (4)$$

$$\eta_\nu = \frac{V''}{V}, \quad (5)$$

$$\xi_\nu^2 = \frac{V'V'''}{V^2}, \quad (6)$$

$$\omega_\nu^3 = \frac{V'^2V''''}{V^3}, \quad (7)$$

where ϵ_ν , η_ν , ξ_ν^2 and ω_ν^3 are called slow-roll parameters, while V is the potential.

In order to compute the CMB power spectrum, we need to calculate the cosmological quantities in terms of the slow-roll parameters as inputs in the `CAMB` cod

$$n_S \simeq 1 - 6\epsilon + 2\eta, \quad (8)$$

$$\alpha_S \simeq 16\eta\epsilon - 24\epsilon^2 - 2\xi^2, \quad (9)$$

$$\beta_S \simeq 192\epsilon^3 - 192\epsilon^2\eta + 32\epsilon\eta^2 + 24\epsilon\xi^2 - 2\eta\xi^2 - 2\omega^3, \quad (10)$$

$$n_T \simeq -2\epsilon, \quad (11)$$

$$\alpha_T \simeq 4\eta\epsilon - 8\epsilon^2, \quad (12)$$

$$r \simeq 16\epsilon. \quad (13)$$

We also need as input the value of the amplitude of the scalar and tensor power spectra, for which we use the value calculated numerically [30].

3. The Starobinsky inflationary model

The Starobinsky inflationary potential was introduced in the 80's by A. Starobinsky [13], this potential is given by

$$V(\phi) = \frac{3}{4}M^2 \left(1 - e^{-\sqrt{2/3}\phi}\right)^2, \quad (14)$$

where $M = 1.13 \times 10^{-5}$ [31] to fit the amplitude of the scalar power spectrum, and ϕ is the inflaton.

From Eqs. (4)–(7) with the potential given by Eq. (14) we calculate analytically the the slow-roll parameters for the Starobinsky inflationary model, and following the notation of Renzi *et al.* [16] we found that they are given by:

$$\epsilon_\nu = \frac{4}{3} \frac{1}{(F_1 - 1)^2}, \quad (15)$$

$$\eta_\nu = -\frac{4}{3} \frac{(F_1 - 2)}{(F_1 - 1)^2}, \quad (16)$$

$$\xi_\nu = \frac{16}{9} \frac{(F_1 - 4)}{(F_1 - 1)^3}, \quad (17)$$

$$\omega_\nu = -\frac{64}{27} \frac{(F_1 - 8)}{(F_1 - 1)^4}, \quad (18)$$

where $F_1 = e\sqrt{\frac{2}{3}}\phi$.

In Fig. 1a we present the CMB angular power spectrum for the Starobinsky inflationary model. The reproduced CMB angular power spectrum shows lower values of temperature fluctuations compared with Planck 2018 results, as is observed in Fig. 1c.

In Fig. 1b is observed the large angular scales ($\ell \lesssim 90$) and its relative error is shown in Fig. 2b. At these scales the contribution to CMB anisotropies are from perturbations that were superhorizon at recombination [32]. In Fig. 1c is observed the intermediate angular scales ($90 < \ell \lesssim 900$) and its relative error is shown in Fig. 2c. In Fig. 1d is observed the large angular scales ($\ell > 900$) and its relative error is shown in Fig. 2d.

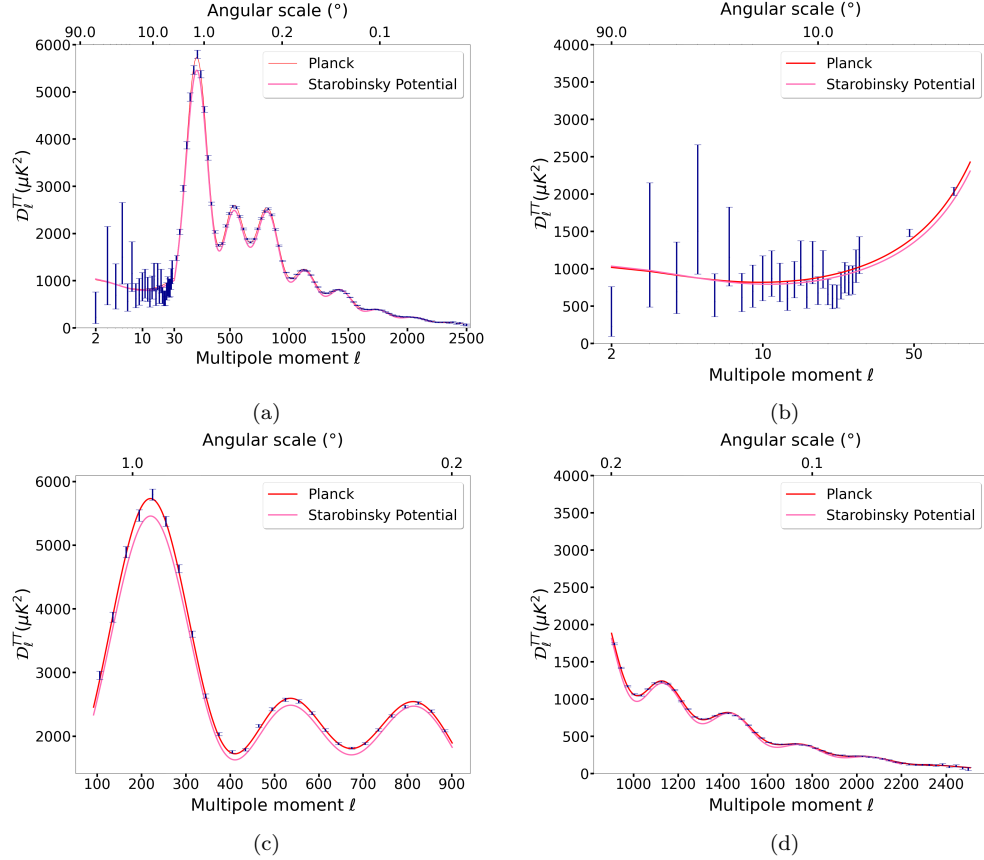


Figure 1: (a) Angular power spectrum for the Starobinsky inflationary model reproduced by CAMB, (b) large angular scales, (c) intermediate angular scales, and (d) small angular scales. Red line: Planck 2018 data with error bars in blue, pink line: CAMB result.

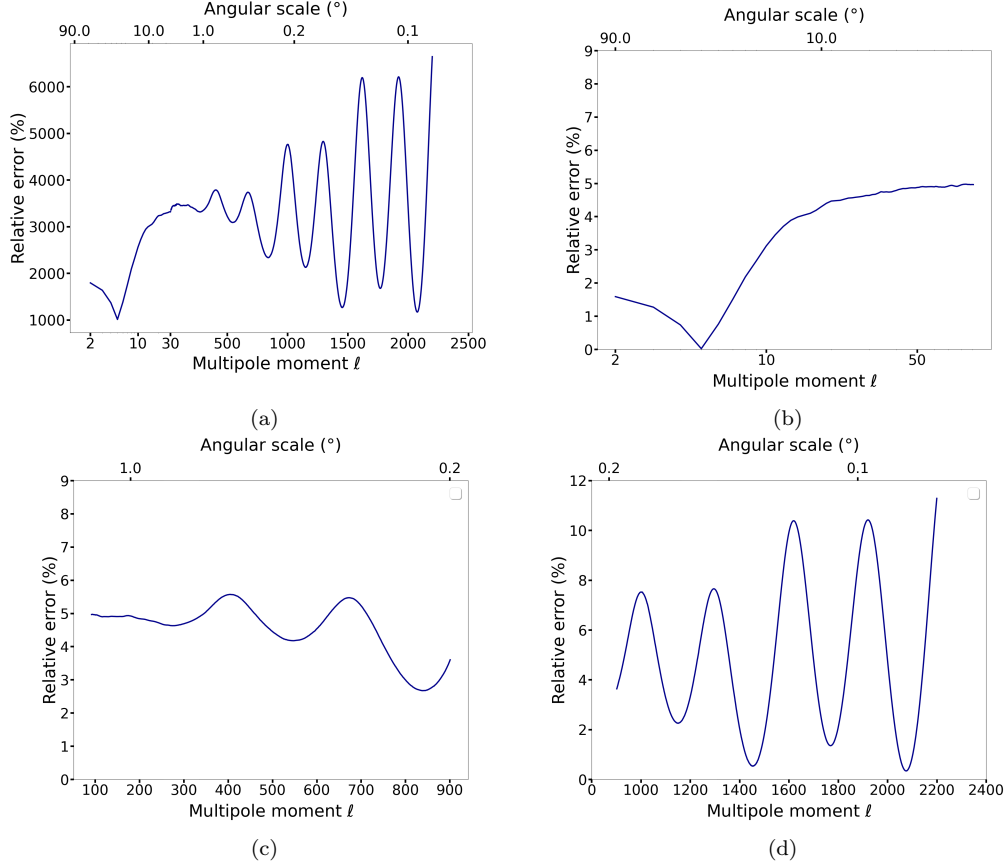


Figure 2: (a) Error of the angular power spectrum for the Starobinsky inflationary model reproduced by CAMB, (b) large angular scales, (c) intermediate angular scales, and (d) small angular scales.

We can easily observe in the relative error plots that the CAMB-reproduced model aligns well with Planck 2018 observations, as indicated by the small errors. However, at smaller angular scales, results exhibit more variability, as evident from the oscillatory behavior of the errors in this section. To assess the overall balance of these errors, let's examine the L2 norm.

When considering all scales, this inflationary model has a L2 norm error of $94 \mu K^2$. At large, intermediate, and small angular scales, the L2 norm errors are $73 \mu K^2$, $146 \mu K^2$, and $37 \mu K^2$, respectively. Therefore, this model reproduces the observational CMB angular spectrum more accurately at smaller angular scales, but the error balance is less favorable at intermediate scales.

Extremum	Starobinsky inflationary model		Planck Satellite	
	Multipole $[\ell]$	Amplitude $[\mu K^2]$	Multipole $[\ell]$	Amplitude $[\mu K^2]$
Peak 1	221	5455.73 ± 0.05	220.6 ± 0.6	5733 ± 39
Trough 1	411	1526.90 ± 0.11	416.3 ± 1.1	1713 ± 20
Peak 2	537	2485.11 ± 0.04	538.1 ± 1.3	2586 ± 23
Trough 2	674	1705.74 ± 0.05	675.5 ± 1.2	1799 ± 14
Peak 3	814	2470.51 ± 0.03	809.8 ± 1.0	2518 ± 17

Table 1: Peaks and troughs of the CMB TT power spectra in the Acoustic Peak region recreated by the Starobinsky inflationary model and reported by Planck satellite.

3.1. The Acoustic Peaks

In Table 1, the acoustic peaks found in the intermediate scale of the spectrum are listed, along with the troughs in this region. We observed that the positions on the multipole axis of the peaks are close to each other for both observed and computed values. Considering the errors of the observed values, all computed peaks, except for the third one, are in agreement with the Planck satellite. The percentage errors of the calculated multipole for peak 1, trough 1, peak 2, trough 2, and peak 3 are 0.18, 1.27, 0.20, 0.22, and 0.52, respectively. However, the differences between the observed and computed amplitudes of the peaks and troughs appear to be greater. The percentage errors of the calculated amplitudes for peak 1, trough 1, peak 2, trough 2, and peak 3 are 4.84, 10.86, 3.90, 5.18, and 1.89, respectively. These errors indicate that, indeed, there is less agreement with the observations in the amplitude of the acoustic peaks than with their multipole.

3.2. Cosmic parameters

In Table 2, some cosmic parameters are calculated theoretically from the Starobinsky inflationary model are compared with their respective observational values from the Planck satellite. Considering the uncertainties, all the parameters are in agreement between their theoretical and observational values.

The percentage errors for the age of the universe, matter density, baryon density, dark energy density, and scalar spectral index are 0.007, 0.16, 0.04, 0.09, and 0.2, respectively. The low percentage errors demonstrate the goodness, accuracy, and precision that the Starobinsky inflationary model exhibits when predicting the observed cosmic parameters.

Cosmic Parameter	Symbol	Starobinsky	Planck
Age of Universe [Gyr]	Age	13.798 ± 0.000	13.797 ± 0.023
Matter density	Ω_m	0.3158 ± 0.0016	0.3153 ± 0.073
Baryon density	$\Omega_b h^2$	0.02238 ± 0.0004	0.02237 ± 0.0001
Dark energy density	Ω_Λ	0.6841 ± 0.0009	0.6847 ± 0.0073
Scalar spectral index	n_S	0.9678 ± 0.0030	0.9649 ± 0.0042

Table 2: Cosmic parameters obtained from the Starobinsky inflationary model compared with the cosmic parameters reported by Planck 2018 results.

4. The generalized Starobinsky inflationary model

The generalized Starobinsky inflationary model is given by [16, 33], and it is a slight modification of the Starobinsky inflationary model

$$V(\phi) = V_0 e^{-2\sqrt{\frac{2}{3}}\phi} \left(e^{\sqrt{\frac{2}{3}}\phi} - 1 \right)^{\frac{2p}{2p-1}}, \quad (19)$$

where p is a real number close to unity, ϕ is the inflaton, and

$$V_0 = 6 \left(\frac{2p-1}{4p} \right) M^2 \left(\frac{1}{2p} \right)^{\frac{1}{2p-1}}. \quad (20)$$

At $p = 1$, equation (19) reduces to the Starobinsky inflationary potential [31, 33]. The value of M is fixed in $M = 1.30 \times 10^{-5}$ in order to obtain the parametrization of the amplitude for the scalar power spectrum at the pivot scale $k = 0.05 \text{ Mpc}^{-1}$ in the Starobinsky inflationary model ($p = 1$) [34].

From Eqs. (4)–(7) using the potential given by Eq. (19), we calculate using Wolfram Mathematica[®] the slow-roll parameters, and following the notation of Renzi [16] we obtain that

$$\epsilon_\nu = \frac{4}{3(2p-1)^2(F_1-1)^2} \left[(1-2p) + (p-1)F_1 \right]^2, \quad (21)$$

$$\eta_\nu = \frac{4}{3(2p-1)^2(F_1-1)^2} \left[(8p^2 - 8p + 2) + (-10p^2 + 13p - 4)F_1 + (2p^2 - 4p + 2)F_1^2 \right], \quad (22)$$

$$\begin{aligned}
\xi_\nu &= \frac{16}{9(2p-1)^4(F_1-1)^4} \left[(64p^4 - 128p^3 + 96p^2 - 32p + 4) \right. \\
&+ (-168p^4 + 380p^3 - 318p^2 + 117p - 16) F_1 + (148p^4 - 388p^3 + 373p^2 - 156p + 24) F_1^2 \\
&+ (-48p^2 + 150p^3 - 173p^2 + 87p - 16) F_1^3 + (4p^4 - 16p^3 + 24p^2 - 16p + 4) F_1^4, \\
&\left. \right] \tag{23}
\end{aligned}$$

$$\begin{aligned}
\omega_\nu &= \frac{64}{27(2p-1)^6(F_1-1)^6} \left[(512p^6 - 1536p^5 + 1920p^4 - 1280p^3 + 480p^2 - 96p + 8) \right. \\
&+ (-2080p^6 + 6736p^5 - 9040p^4 + 6440p^3 - 2570p^2 + 545p - 48) F_1 \\
&+ (3328p^6 - 11744p^5 + 17088p^4 - 13136p^3 + 5632p^2 - 1278p + 120) F_1^2 \\
&+ (-2632p^6 + 10236p^5 - 16350p^4 + 13741p^3 - 6414p^2 + 1578p - 160) F_1^3 \\
&+ (1048p^6 - 4536p^5 + 8070p^4 - 7552p^3 + 3920p^2 - 1070p + 120) F_1^4 \\
&+ (-184p^6 + 900p^5 - 1822p^4 + 1953p^3 - 1168p^2 + 369p - 48) F_1^5 \\
&\left. + (-2632p^6 + 10236p^5 - 16350p^4 + 13741p^3 - 6414p^2 + 1578p - 160) F_1^6 \right]. \tag{24}
\end{aligned}$$

Fig. 3 displays the CMB angular spectrum reproduced in **CAMB** for various values of the parameter p in comparison to Planck 2018 data. It is evident that for $p > 1$, this parameter shifts the spectrum upwards, whereas for $p < 1$ it shifts it downwards in comparison to the Starobinsky inflationary model ($p = 1$). As the reproduced CMB by the Starobinsky inflationary model was under the observational data, we expect the optimal value of p to be a little bit greater than 1 to make it approach the observational curve.

Performing the **CAMB** reproduction of the CMB for various values of p , we found that the value that gives us the best tensor-to-scalar ratio r and the scalar spectral index n_s , in comparison with the ones reported by Planck 2018 results, is 1.0004 ± 0.0001 , which is greater than 1 as predicted before. Now let us plot it.

In Fig. 4b is observed the large angular scales ($\ell \lesssim 90$) at $p = 1.0004$ and its relative error is shown in Fig. 5b. In Fig. 4c is observed the intermediate angular scales ($90 < \ell \lesssim 900$) at $p = 1.0004$ and its relative error is shown in Fig. 5c. In Fig. 4d is observed the large angular scales ($\ell > 900$) at $p = 1.0004$ and its relative error is shown in Fig. 5d.

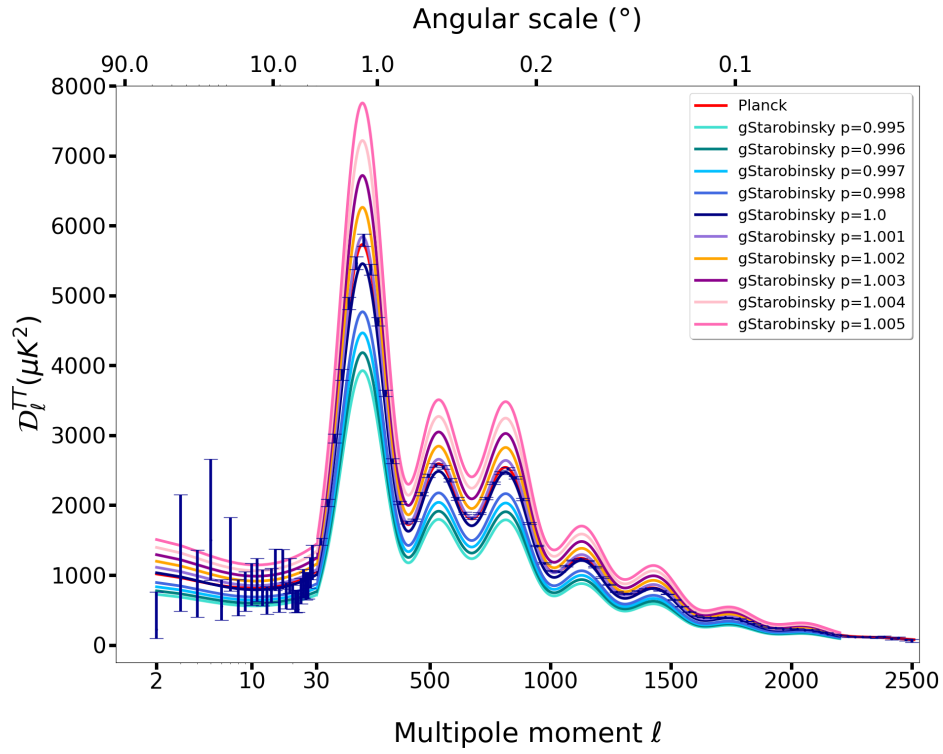


Figure 3: Angular power spectrum for the generalized Starobinsky inflationary model reproduced by CAMB for different values of p . Red solid line: Planck 2018 data.

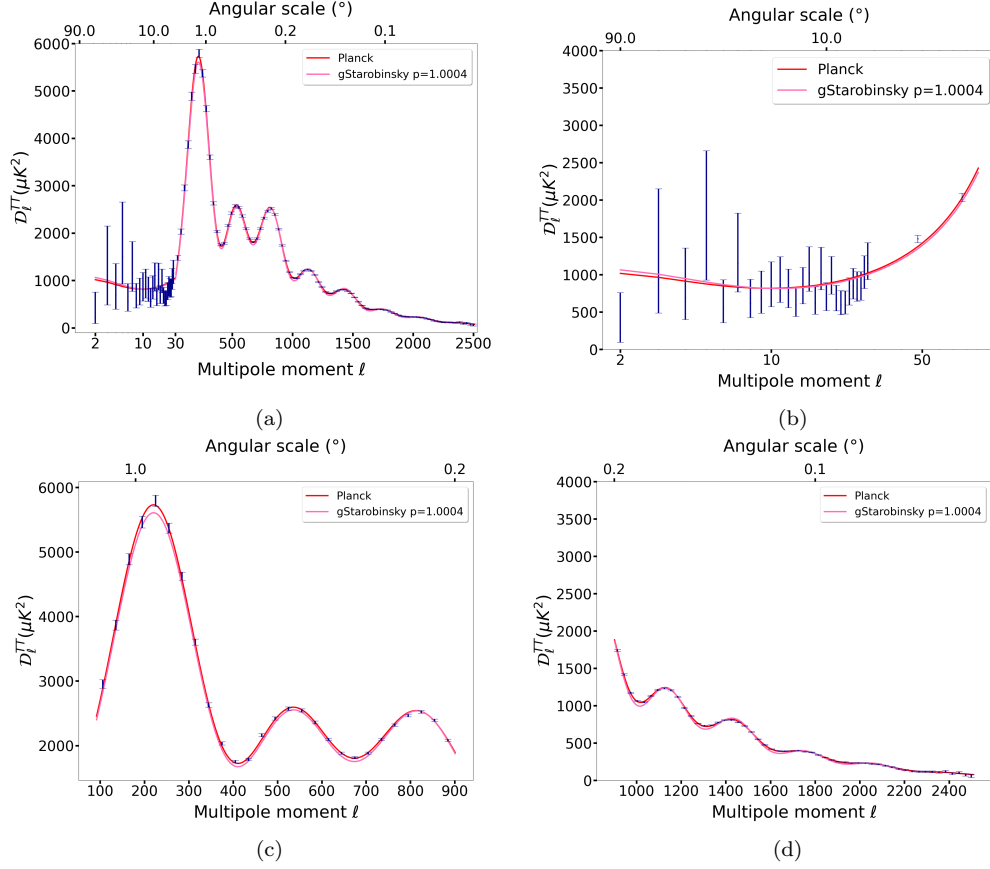


Figure 4: (a) Angular power spectrum for the generalized Starobinsky inflationary model reproduced by **CAMB** for $p = 1.0004$, (b) large angular scales, (c) intermediate angular scales, and (d) small angular scales. Red line: Planck 2018 data with error bars in blue, pink line: **CAMB** result.

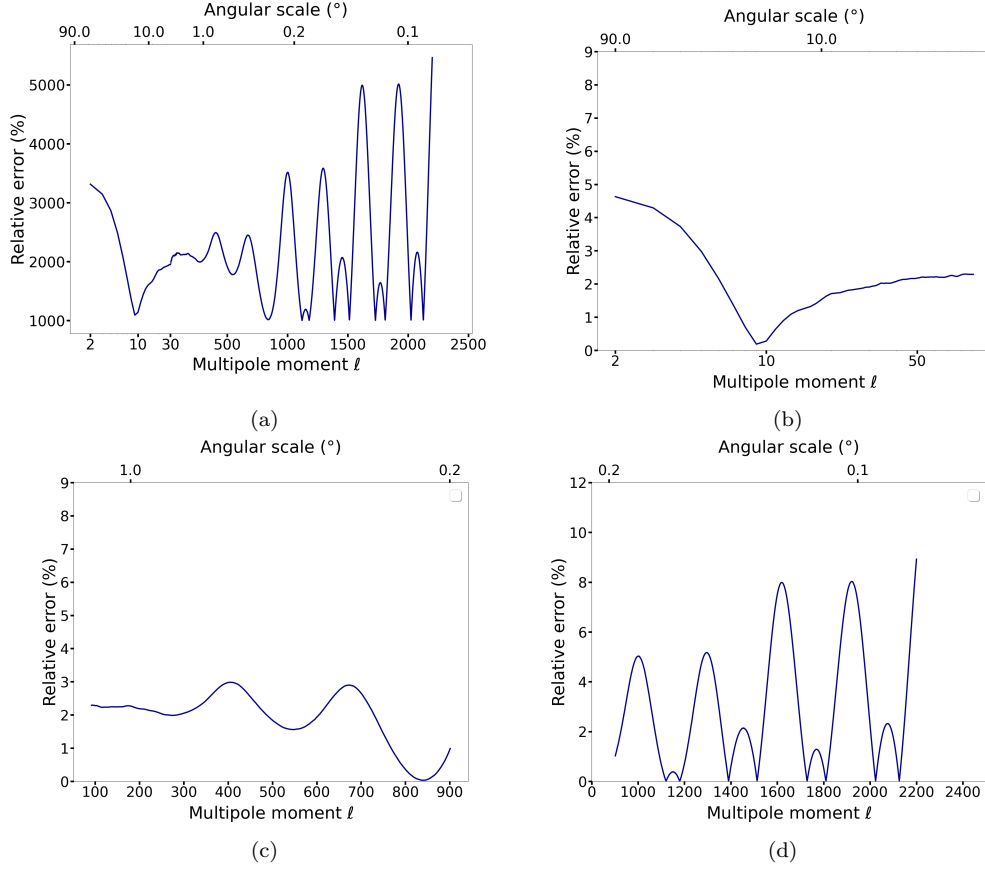


Figure 5: (a) Error of the angular power spectrum for the generalized Starobinsky inflationary model reproduced by **CAMB** for $p = 1.0004$, (b) large angular scales, (c) intermediate angular scales, and (d) small angular scales.

Extremum	Generalized Starobinsky inflationary model		Planck Satellite	
	Multipole $[\ell]$	Amplitude $[\mu K^2]$	Multipole $[\ell]$	Amplitude $[\mu K^2]$
Peak 1	221	5607.40 ± 0.02	220.6 ± 0.6	5733 ± 39
Trough 1	411	1671.43 ± 0.03	416.3 ± 1.1	1713 ± 20
Peak 2	537	2552.95 ± 0.01	538.1 ± 1.3	2586 ± 23
Trough 2	674	1752.16 ± 0.03	675.5 ± 1.2	1799 ± 14
Peak 3	814	2537.55 ± 0.00	809.8 ± 1.0	2518 ± 17

Table 3: Peaks and troughs of the CMB TT power spectra in the Acoustic Peak region recreated by the generalized Starobinsky inflationary model for $p = 1.0004$ and reported by Planck satellite.

For $p = 1.0004$, this **CAMB**-reproduced model aligns well with Planck 2018 observations, even surpassing the Starobinsky inflationary model, as evidenced by the smaller errors it exhibits in comparison. Variability in the results persists at small angular scales as in the previous model. To assess the overall balance of these errors, let us examine the L2 norm.

When considering all scales, this inflationary model has an L2 norm error of $43 \mu K^2$. At large, intermediate, and small angular scales, the L2 norm errors are $34 \mu K^2$, $65 \mu K^2$, and $22 \mu K^2$, respectively. Therefore, similar to the Starobinsky inflationary model, the generalized Starobinsky inflationary model reproduces the observational CMB angular spectrum more accurately at smaller angular scales, but the error balance is less favorable at intermediate scales. However, it significantly outperforms the Starobinsky inflationary model both in terms of relative error size and error balance

4.1. The Acoustic Peaks

In Table 3, we present the acoustic peaks identified in the intermediate range of the spectrum, along with the corresponding troughs. Our observations reveal close proximity in the positions along the multipole axis between the observed and calculated values. Considering the uncertainties associated with the observed data, all computed peaks, with the exception of the third one, align well with the Planck satellite. The percentage errors associated with the calculated multipole values for peak 1, trough 1, peak 2, trough 2, and peak 3 are 0.18, 1, 27, 0.20, 0.22, and 0.52, respectively. These errors are exactly the same as those reported by the Starobinsky inflationary model.

On the other hand, the percentage errors for the calculated amplitudes

Cosmic Parameter	Symbol	G. Starobinsky	Planck
Age of Universe [Gyr]	Age	13.798 ± 0.000	13.797 ± 0.023
Matter density	Ω_m	0.3158 ± 0.0016	0.3153 ± 0.073
Baryon density	$\Omega_b h^2$	0.02238 ± 0.0004	0.02237 ± 0.0001
Dark energy density	Ω_Λ	0.6841 ± 0.0009	0.6847 ± 0.0073
Scalar spectral index	n_s	0.9672 ± 0.0024	0.9649 ± 0.0042

Table 4: Cosmic parameters obtained from the generalized Starobinsky inflationary model with $p = 1.0004$ compared with the cosmic parameters reported by Planck 2018 results.

of peak 1, trough 1, peak 2, trough 2, and peak 3 are 2.20, 2.43, 1.28, 2.60, and 0.78, respectively. These errors once again indicate that there is less agreement with the observations in terms of the amplitude of the acoustic peaks compared to their multipole positions. Nevertheless, these errors are significantly smaller than those from the Starobinsky inflationary model.

4.2. Cosmic Parameters

In Table 4, we compare certain cosmic parameters computed theoretically using the generalized Starobinsky inflationary model with their corresponding observational values derived from the Planck satellite. Once again, all parameters demonstrate alignment between their theoretical predictions and observed values. In fact, all values remain the same as those derived from the Starobinsky model ($p = 1$), except for the scalar spectral index, which has a smaller uncertainty this time.

The percentage errors associated with the age of the universe, matter density, baryon density, dark energy density, and scalar spectral index are 0.007, 0.16, 0.04, 0.09, and 0.2, respectively. This model exhibits the same capacity for accurate and precise predictions of the observed cosmic parameters as the Starobinsky inflationary model. However, due to the smaller uncertainty in the scalar spectral index, we can say that this generalized model is slightly better in that aspect, although the difference is not significant.

5. Chaotic inflationary model with a step

The chaotic inflationary model with a step was introduced by Adams [22], and it is given by

$$V(\phi) = \frac{1}{2}m^2\phi^2 \left[1 + c \tanh \left(\frac{\phi - \phi_{\text{step}}}{d} \right) \right], \quad (25)$$

where the step occurs at $\phi = \phi_{\text{step}}$, ϕ is the inflaton, m is the inflaton mass, and the parameters c and d are related to the amplitude and width of the feature, respectively [18, 19, 20, 21, 22].

Using Eqs. (4)–(7) we calculated also using Wolfram Mathematica[®] the slow-roll parameters for the potential (25) of the chaotic inflationary model with a step, obtaining

$$\epsilon_\nu = \frac{1}{2\phi^2} \left[\frac{c\phi F_2^2 + 2(d + c d F_3)}{d^2(1 + c F_3)} \right]^2, \quad (26)$$

$$\eta_\nu = \frac{2}{\phi^2} \left[1 + \frac{c\phi F_2^2(2d - \phi F_3)}{d^2(1 + c F_3)} \right], \quad (27)$$

$$\xi_\nu = \frac{2}{\phi^3} F_2^2 [c\phi F_2^2 + 2(d + c d F_3)] \left[\frac{(3d^2 + 2\phi^2 - 3\phi F_2^2)(\phi + d F_4)}{d^4(1 + c F_3)^2} \right] \quad (28)$$

$$\omega_\nu = -\frac{8c}{\phi^4} (d - \phi F_3) (-\phi + 3F_2^2 + 3d F_3) \left[\frac{c\phi F_2^3 + 2F_2(d + c d F_3)^2}{d^6(1 + c F_3)^3} \right], \quad (29)$$

where

$$F_2 = \text{sech} \left(\frac{\phi - \phi_{\text{step}}}{d} \right), \quad (30)$$

$$F_3 = \tanh \left(\frac{\phi - \phi_{\text{step}}}{d} \right), \quad (31)$$

$$F_4 = \sinh \left[\frac{2(\phi - \phi_{\text{step}})}{d} \right]. \quad (32)$$

Fig. 6 shows the CMB angular power spectrum for the chaotic inflationary model with a step, different values of the parameters c and d were used to reproduce different spectra using CAMB. In Fig. 7a we report the best fit

compared to Planck 2018 data, for this fit we use $d = 0.04$ and $c = 0.12$. Our best fit was chosen by computing the relative error between our model and Planck 2018 data and selecting the parameters that produce the lower relative error. We can see from Fig. 8a that the relative error found for these parameters is lower than 9% concerning the spectrum from Planck 2018 data.

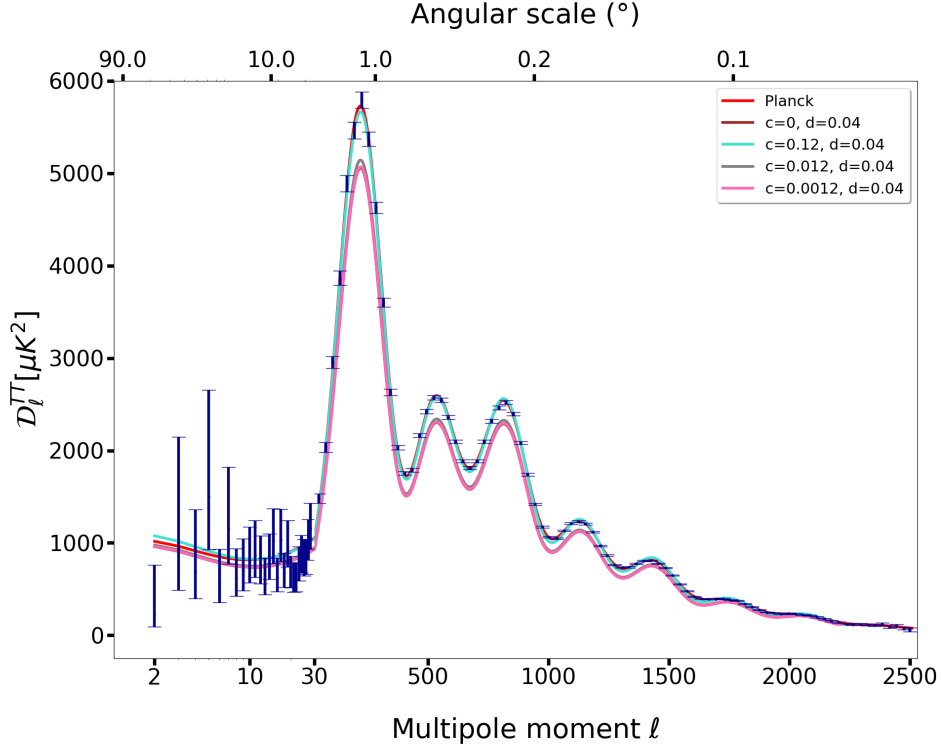


Figure 6: Angular power spectrum for the chaotic inflationary model with a step reproduced by **CAMB** for different values of c and d . Red line: Planck 2018 data, brown line: result for $c = 0$, turquoise line: result for $c = 0.12$ and $d = 0.04$, gray line: result for $c = 0.012$ and $d = 0.04$, and pink line: result for $c = 0.0012$ and $d = 0.04$.

In Fig. 7b is observed the large angular scales ($\ell < 90$) at $c = 0.12$ and $d = 0.04$, and its relative error is shown in Fig. 8b. In Fig. 7c is observed the intermediate angular scales ($90 < \ell \lesssim 900$) at $c = 0.12$ and $d = 0.04$, and its relative error is shown in Fig. 8c. In Fig. 7d is observed the large angular scales ($\ell > 900$) at $c = 0.12$ and $d = 0.04$, and its relative error is shown in Fig. 8d.

Extreme	Inflationary Chaotic model with a step		Planck Satellite	
	Multipole $[\ell]$	Amplitude $[\mu K^2]$	Multipole $[\ell]$	Amplitude $[\mu K^2]$
Peak 1	221	5143.42 ± 0.10	220.6 ± 0.6	5733 ± 39
Trough 1	411	1532.55 ± 0.11	416.3 ± 1.1	1713 ± 20
Peak 2	537	2340.94 ± 0.10	538.1 ± 1.3	2586 ± 23
Trough 2	674	1606.23 ± 0.11	675.5 ± 1.2	1799 ± 14
Peak 3	814	2326.50 ± 0.08	809.8 ± 1.0	2518 ± 17

Table 5: Peaks and troughs of the CMB TT power spectra in the Acoustic Peak region recreated by the chaotic inflationary model with a step for $p = 1.0004$ and reported by Planck satellite.

This model reproduces a CMB that aligns better with the Planck 2018 observations, surpassing the Starobinsky and Generalized Starobinsky inflationary models. High-variability in the results persists at small angular scales as in the previous models. To assess the overall balance of these errors, let's examine the L2 norm.

When considering all scales, this inflationary model has a L2 norm error of $26 \mu K^2$. At large, intermediate, and small angular scales, the L2 norm errors are $20 \mu K^2$, $36 \mu K^2$, and $18 \mu K^2$, respectively. Therefore, the chaotic model exhibits similar characteristics as the models seen until now. It reproduced the CMB angular spectrum more accurately at smaller angular scales, but the error balance is less favorable at intermediate scales. But, in general, it is the best model for reproducing the CMB angular spectrum, both in terms of relative error size and error balance.

5.1. The Acoustic Peaks

In Table 5, we present the acoustic peaks identified in the intermediate scale of the spectrum, along with the corresponding troughs in this range.

Once again, our observations reveal proximity between the positions on the multipole axis of both observed and computed peaks. Taking into account the errors associated with the observed values, all computed peaks, except the third one, align well with the data from the Planck satellite. Specifically, the percentage errors for the calculated multipole values corresponding to peak 1, trough 1, peak 2, trough 2, and peak 3 are 0.18, 1.27, 0.20, 0.22, and 0.52, respectively. We can see again the same percentage error of the previously presented models.

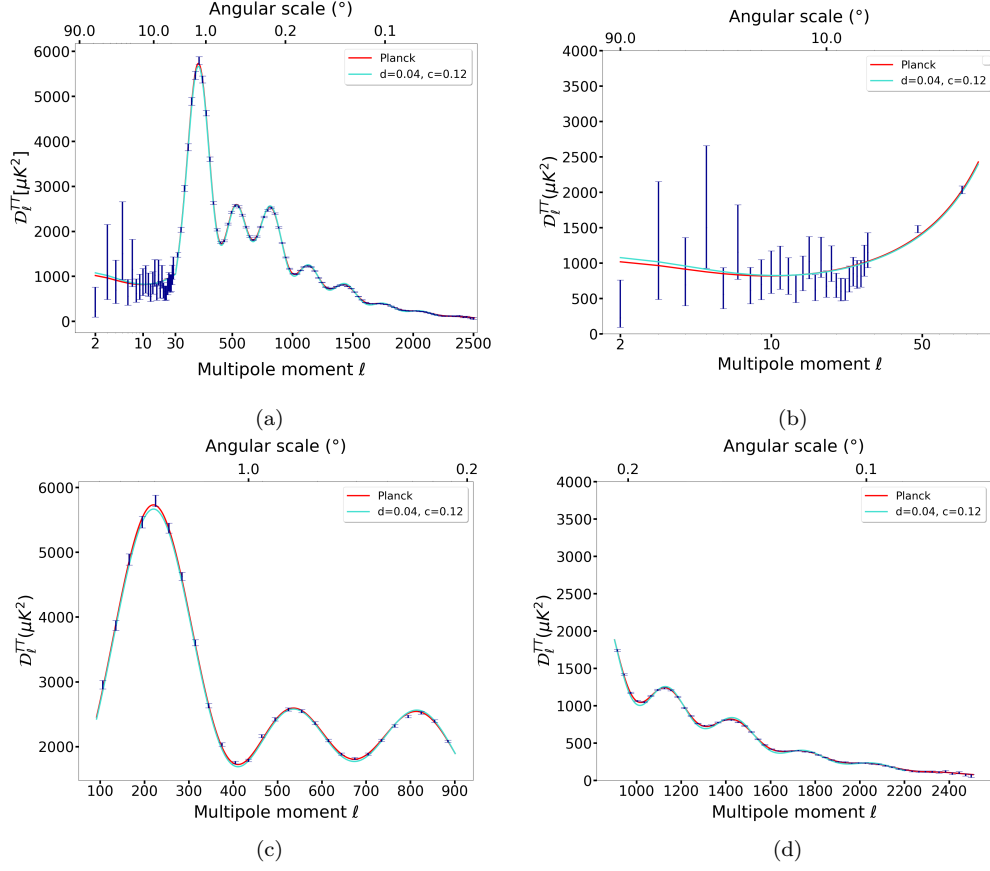


Figure 7: (a) Angular power spectrum for the chaotic inflationary model with a step reproduced by CAMB for $c = 0.12$ and $d = 0.04$, (b) large angular scales, (c) intermediate angular scales, and (d) small angular scales. Red line: Planck 2018 data with error bars in blue, turquoise line: CAMB result.

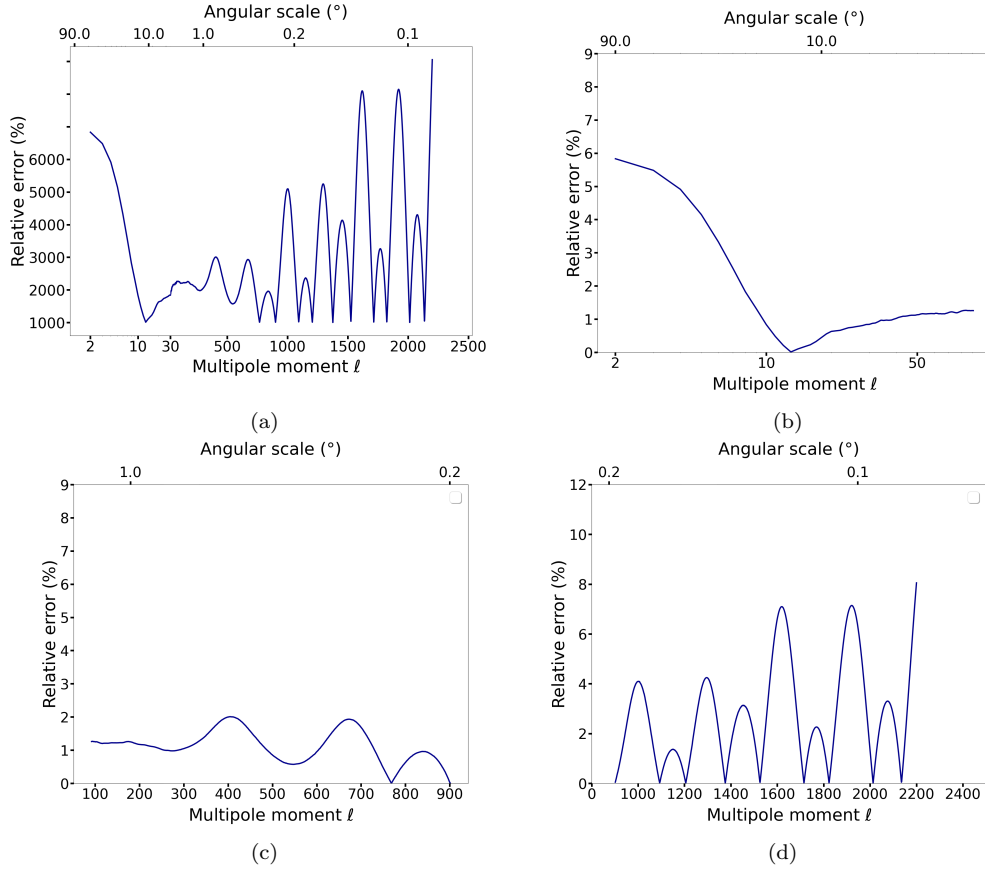


Figure 8: (a) Error of the angular power spectrum for the chaotic inflationary model with a step reproduced by CAMB, (b) large angular scales, (c) intermediate angular scales, and (d) small angular scales.

The percentage errors for the calculated amplitudes of peak 1, trough 1, peak 2, trough 2, and peak 3 are 10.28, 10.53, 9.48, 10.72, and 7.61, respectively. Once again, there is less agreement between the observations and the computed values in terms of the amplitude of the acoustic peaks compared to their multipole positions. Although the computed data generally fits better with the observations than the previous models, it exhibits greater percentage errors when comparing the acoustic peaks in the intermediate angular scale of the spectrum.

5.2. Cosmic Parameters

In Table 6, we once again analyze the same cosmic parameters derived theoretically from the chaotic model and compare them with their corresponding observational values obtained from the Planck satellite. Considering uncertainties, all the parameters exhibit alignment between their theoretical and observational values.

Cosmic Parameter	Symbol	Chaotic	Planck
Age of Universe [Gyr]	Age	13.798 ± 0.000	13.797 ± 0.023
Matter density	Ω_m	0.3158 ± 0.0016	0.3153 ± 0.073
Baryon density	$\Omega_b h^2$	0.02238 ± 0.0004	0.02237 ± 0.0001
Dark energy density	Ω_Λ	0.6841 ± 0.0009	0.6847 ± 0.0073
Scalar spectral index	n_s	0.9669 ± 0.0021	0.9649 ± 0.0042

Table 6: Cosmic parameters obtained from the chaotic inflationary model with a step for $p = 1.0004$ compared with the cosmic parameters reported by Planck 2018 results.

The percentage errors for the age of the universe, matter density, baryon density, dark energy density, and scalar spectral index are 0.007, 0.16, 0.04, 0.09, and 0.2, respectively. The effectiveness, accuracy, and precision demonstrated by the chaotic model are again similar to the previous ones. It can also be stated that it is slightly better, mainly due to the better precision it achieves when predicting the scalar spectral index.

6. Conclusions

In summary, this article explores and analyzes three different inflationary models: the Starobinsky inflationary model, the generalized Starobinsky inflationary model, and the chaotic inflationary model with a step.

For the Starobinsky inflationary model, the inflationary potential is given by Eq. (14), and the slow-roll parameters are calculated analytically. The CMB angular power spectrum for this model is presented and compared with Planck 2018 data in various plots, showing good agreement at small angular scales but with larger errors at intermediate scales. The acoustic peaks and troughs are also listed, and cosmic parameters calculated from the model are compared with observational values, demonstrating overall agreement.

The generalized Starobinsky inflationary model, described by Eq. (19), introduces an additional parameter p , and the slow-roll parameters are derived. The CMB angular power spectrum for various values of p is presented, and the optimal value that best fits the Planck 2018 data is determined to be $p = 1.0004 \pm 0.0001$. The model exhibits improved performance compared to the original Starobinsky inflationary model, with smaller errors in the relative error plots. The acoustic peaks and cosmic parameters are also analyzed, showing good agreement with observations.

Finally, the chaotic inflationary model with a step, described by Eq. (25), is investigated. The slow-roll parameters are derived, and the CMB angular power spectrum is presented. The model introduces a step in the potential, and its impact on the power spectrum is analyzed. The model is characterized by parameters such as m , c , d , and ϕ_{step} .

Overall, all three inflationary models successfully replicate the shape of the temperature power spectrum of the CMB while aligning with the values of cosmic parameters. However, the chaotic inflationary model with a step produce better results in the positioning and amplitudes of the peaks and troughs. The article concludes by summarizing the key findings and comparing the performance of the three models in reproducing the observed CMB angular spectrum, highlighting their strengths and limitations.

7. Acknolegments

We want to thanks to Professor Antony Lewis for your help always answering my question in his CosmoCoffee forum, and to Professor Victor Miralles for useful discussions about the use of **CAMB** code.

References

- [1] R. A. Alpher, and R. Herman. Evolution of the Universe. *Nature*, 162(4124):774, 1948.

- [2] A. A. Penzias, and R. W. Wilson. A measurement of excess antenna temperature at 4080 Mc/s. *ApJ*, 142:419, 1965.
- [3] R. Tojeiro. Understanding the Cosmic Microwave Background Temperature Power Spectrum, 2006.
- [4] Ruth Durrer. The cosmic microwave background: the history of its experimental investigation and its significance for cosmology. *Class. Quantum Grav.*, 32:124007, 2015.
- [5] A. H. Guth. Inflationary universe: A possible solution to the horizon and flatness problems. *Phy. Rev. D*, 23:347, 1981.
- [6] D. Pozo, J. Zambrano, I. Villegas, R. Hernández-Jiménez, and C. Rojas. Some inflationary models under the light of Planck 2018 results. *Astropart. Phys.*, 2024.
- [7] Y. Akrami *et al.* Planck 2018 results-X. Constraints on inflation. *A&A*, 641:A10, 2020.
- [8] J. Martin, C. Ringeval, R. Trotta, and V. Vennin. The best inflationary models after Planck. *JCAP*, 2014:039, 2014.
- [9] J. Martin, and C. Ringeval. Inflation after WMAP3: confronting the slow-roll and exact power spectra with CMB data. *JCAP*, 24:009, 2006.
- [10] Antony Lewis, Anthony Challinor, and Anthony Lasenby. Efficient computation of CMB anisotropies in closed FRW models. *Astrophys. J.*, 538, 2000.
- [11] Cullan Howlett, Antony Lewis, Alex Hall, and Anthony Challinor. CMB power spectrum parameter degeneracies in the era of precision cosmology. *JCAP*, 1204, 2012.
- [12] N. Aghanim *et al.* Planck 2018 results–I, Overview and the cosmological legacy of Planck. *A&A*, 641:A1, 2020.
- [13] A. A. Starobinsky. A new type of isotropic cosmological models without singularity. *Phys. Lett. B*, 91:99, 1980.

- [14] C. Rojas. Study of scalar and tensor power spectra in the generalized Starobinsky inflationary model using semiclassical methods. *Astroparticle Physics*, 143:102745, 2022.
- [15] S. Meza, D. Altamirano, M. Z. Mughal, and C. Rojas. Numerical analysis of the generalized Starobinsky inflationary model. *Int. J. Mod. Phys. D*, 30:2150062, 2021.
- [16] F. Renzi, M. Shokri, and A. Melchiorri. What is the amplitude of the gravitational waves background expected in the Starobinsky model? *Phys. Dark. Univ.*, 27:100450, 2020.
- [17] E. Di Valentino, and L. Mersini–Houghton. Testing predictions of the quantum landscape multiverse 1: the Starobinsky inflationary potential. *JCAP*, 03:100650, 2017.
- [18] R. Thomas, J. Thomas, and M. Joy. Primordial gravitational waves by chaotic potential with a sharp step. *Phys. Dark. Univ.*, 42, 2023.
- [19] C. Rojas, and R. Hernandez–Jiménez. Inflation from a chaotic potential with a step. *Phys. Dark Univ.*, 40:101188, 2023.
- [20] A. G Cadavid. Features in single field slow–roll inflation. *J. Phys.: Conf. Ser.*, 831:012003, 2017.
- [21] A. G. Cadavid, and A. E. Romano. Effects of discontinuities of the derivatives of the inflaton potential. *Eur. Phys. J. C*, 75:589, 2015.
- [22] J. Adams, B. Cresswell, and R. Easter. Inflationary perturbations from a potential with a step. *Phys. Rev. D*, 64:123514, 2001.
- [23] A. de la Macorra, J. Garrido, and E. Almaraz. Towards a Solution to the H_0 Tension: the Price to Pay. *Phys. Rev. D*, 105:023526, 2022.
- [24] U. Purkayastha, V. Sudevan, and R. Saha. Aforegroundmodelindependentestimation of joint posterior of CMB E-mode polarization over large angular scales. *Mod. Phys. Lett. A*, 37, 2022.
- [25] S. Serjeant. *Observational cosmology*. Cambridge University Press, 2010.
- [26] A. Liddle. *An introduction to modern cosmology, 3rd Edition*. John Wiley & Sons, 2015.

- [27] D. Scott and G. Scot Smoot. Cosmic background radiation mini-review. *astro-ph/0406567*, 2004.
- [28] C. I. Lazaroui. On the slow roll expansion of one-field cosmological models. *Nuc. Phys. B*, 1000, 2024.
- [29] M. Zarei. On the running of the spectral index to all orders: a new model-dependent approach to constrain inflationary models. *Class. Quantum Grav.*, 33:115008, 2016.
- [30] T. Tapia, M. Z. Mughal, and C. Rojas. Semiclassical analysis of the Starobinsky inflationary model. *Phys. Dark. Univ.*, 30:100650, 2020.
- [31] A. V. Toporensky S. S. Mishra, V. Sahni. Initial conditions for inflation in an FRW Universe. *Phys. Rev. D*, 98(8), 2018.
- [32] D. S. Gorbunov, and V. A. Rubakov. *Introduction to the theory of the Early Universe: Cosmological Perturbations and Inflationary Theory*. World Scientific, 2011.
- [33] J. Martin, C. Ringeval, and V. Vennin. Encyclopaedia Inflationaris. *Phys. Dark Univ.*, 5-6:75, 2014.
- [34] D. D. Canko, I. D. Gialamas, and G. P. Kodaxis. A simple $F(\mathcal{R}, \phi)$ deformation of Starobinsky inflationary model. *Eur. Phys. J. C.*, 80:458, 2020.